

High-spin studies of ^{219}Ac

F. Cristancho, J. X. Saladin, and M. P. Metlay
University of Pittsburgh, Pittsburgh, Pennsylvania 15260

W. Nazarewicz*

*Joint Institute for Heavy Ion Research, Oak Ridge National Laboratory, P.O. Box 2008, Oak Ridge, Tennessee 37831
 and Department of Physics, University of Tennessee, Knoxville, Tennessee 37996*

C. Baktash, M. Halbert, I-Y. Lee,[†] and D. F. Winchell[‡]
Physics Division, Oak Ridge National Laboratory, Oak Ridge, Tennessee 37831

S. M. Fischer
University of Notre Dame, Notre Dame, Indiana 46556

M. K. Kabadiyski
II. Physikalisches Institut, Universität Göttingen, Bunsenstr. 7-9, 3400 Göttingen, Federal Republic of Germany
 (Received 16 September 1993)

High-spin states up to a probable spin $I = \frac{45}{2}$ have been investigated in ^{219}Ac using the reaction $^{209}\text{Bi} (^{13}\text{C}, 3n)$. The alternating-parity sequences already observed up to $I = \frac{31}{2}$ do not seem to develop further at higher spins. A new sideband was observed as well as several $E2/M1$ transitions linking the states of positive parity. Multipolarities and mixing ratios were deduced from an analysis of DCO ratios. In addition mixing ratios were obtained independently from the branching ratios. This allowed for determination of $B(M1)/B(E2)$ ratios up to $I^\pi = \frac{29}{2}^+$. The data are discussed in terms of a transition from the weak coupling scheme at low and medium spins to the particle-hole regime for $I \gtrsim \frac{31}{2}$.

PACS number(s): 21.60.Ev, 23.20.Gq, 23.20.Lv, 27.80.+w

I. INTRODUCTION

The study of light odd- A actinide isotopes is of considerable interest, since there is strong evidence for the presence of either static or dynamic octupole deformations [1]. This evidence comes from the experimental observation of alternating-parity rotational bands, enhanced $E1$ transitions, and the presence of parity doublets, which are associated with the breaking of the intrinsic reflection symmetry.

There exist several theoretical investigations of these nuclei based on a rigidly deformed reflection-asymmetric rotor plus quasiparticle model [2,3]. The low-energy one-quasiparticle excitations have recently been studied in Ref. [4] using a mean-field approach based on a reflection-asymmetric potential. As one approaches the neutron shell closure at $N=126$, the collective phenomena dominating at neutron numbers around and above $N=132$ seem to vanish into single-particle struc-

tures. There is a narrow region of nuclei centered around $N=130$ [5-7] which still show a considerable degree of collectivity, but in which one expects to see the interplay between collective octupole and quadrupole excitations on one hand and spherical shell model structures on the other. In the present work we study the transitional nucleus ^{219}Ac . Previous experiments have been performed [8,9] on this nucleus using techniques similar to those used here. The aim of our investigation was to extend the level scheme to higher spins and, in particular, to search for the existence of parity doublets at higher spins and excitation energies. We were also able to resolve a discrepancy between the two previous experiments.

During the preparation of this paper, it came to our attention that the Notre Dame-Argonne collaboration has also studied this nucleus. Their level scheme [10] also shows some of the new high-lying transitions, as well as a similar sideband structure. There are, however, some new transitions in Ref. [10] which we do not see in our data and some transitions whose assignments are in conflict with our data.

II. EXPERIMENT AND DATA ANALYSIS

High-spin states in ^{219}Ac were populated via the $^{209}\text{Bi}(^{13}\text{C}, 3n)$ reaction at 67 MeV, using a 5 mg cm^{-2} target. The experiment was carried out at the HHIRF

*Permanent address: Institute of Theoretical Physics, Warsaw University, Hoza 69, 00-681 Warsaw, Poland; Institute of Physics, Warsaw Institute of Technology, Warsaw, Poland.

[†]Present address: Nuclear Science Division, Lawrence Berkeley Laboratory, Berkeley, CA 94720.

[‡]Present address: Physics Department, University of Pennsylvania, Philadelphia, PA 19109.

Laboratory at Oak Ridge. γ rays were detected with the Spin Spectrometer [11] in a configuration consisting of 50 NaI and 19 Compton-suppressed Ge detectors. Doppler-shift-corrected energies of the Ge detectors, the energies of the NaI detectors, and their fold k (number of detectors that fired), as well as timing data, were recorded in an event-by-event mode. Data with fold ≥ 5 were sorted off line into several two-dimensional matrices of γ -ray

energies in order either to construct the level scheme or to obtain directional correlation from oriented states (DCO) ratios. A total of 140×10^6 γ - γ coincidences were obtained. Energy and efficiency calibrations were carried out with standard radioactive sources (^{152}Eu and ^{133}Ba).

Multipolarity assignments were derived from DCO ratios. We define the DCO ratio of the transition γ_1 and gating transition γ_2 as

$$R(\text{DCO}) = \frac{Y[\gamma_1 \text{ at } (63^\circ, 117^\circ), \text{ gated with } \gamma_2 \text{ at } (24^\circ, 156^\circ)]}{Y[\gamma_1 \text{ at } (24^\circ, 156^\circ), \text{ gated with } \gamma_2 \text{ at } (63^\circ, 117^\circ)]} \quad (1)$$

In this work γ_2 represents a single or a group of stretched $E2$ transitions. The intensity Y is corrected for the efficiency of all of the involved transitions. The angles are measured with respect to the beam axis. In

the following, when referring to a specific $R(\text{DCO})$ value, we will specify the γ_1 transition only whenever it does not introduce ambiguities.

Table I shows transition energies, initial and final spins,

TABLE I. Energies (E_γ), initial and final spins (I_i, I_f), relative intensities (I_γ), and DCO ratios [$R(\text{DCO})$] for the transitions assigned to ^{219}Ac in the present work. The last column gives the transitions used as gates [γ_2 of Eq. (1)] to obtain the corresponding $R(\text{DCO})$.

E_γ (keV)	I_i	I_f	I_γ	R (DCO)	Gate(s) ^a
57.24(3)	$\frac{17}{2}^-$	$\frac{15}{2}^-$	19.2(6)	0.86(9)	C
80.86(2)	$\frac{15}{2}^-$	$\frac{13}{2}^+$	6.1(3)	0.74(22)	B
106.01(2) ^b	$\frac{33}{2}^+$	$\frac{31}{2}^-$			
111.67(11)	$\frac{21}{2}^+$	$(\frac{19}{2}^-)$	4.6(5)		
125.43(3)	$\frac{31}{2}^+$	$\frac{29}{2}^-$	5.1(2)	0.73(8)	A
133.27(1)	$\frac{25}{2}^+$	$\frac{23}{2}^-$	17.7(2)	0.68(2)	B
146.53(6)	$\frac{29}{2}^+$	$\frac{27}{2}^-$	15.4(22)	0.67(2)	A
147.26(16)	$\frac{27}{2}^+$	$\frac{25}{2}^-$	5.4(21)		
150.99(2) ^c	$\frac{19}{2}^-$	$\frac{17}{2}^+$	26.0(25)	0.69(2)	A
150.78(5)	$\frac{21}{2}^-$	$\frac{19}{2}^+$	14.3(24)		
156.44(6)	$(\frac{33}{2}^-)$	$\frac{31}{2}^-$	2.4(3)	0.76(12)	B
158.74(8)	$\frac{25}{2}^+$	$(\frac{23}{2}^-)$	3.2(3)	0.97(35)	C
165.29(1)	$\frac{21}{2}^+$	$\frac{19}{2}^-$	34.2(5)	0.67(2)	C
185.02(1)	$\frac{23}{2}^+$	$\frac{21}{2}^-$	24.2(5)	0.63(14)	A
209.01(1)	$\frac{17}{2}^+$	$\frac{15}{2}^-$	41.3(3)	0.68(2)	C
217.87(23)	$\frac{21}{2}^+$	$\frac{19}{2}^+$	4.3(15)	0.83(7)	A
221.63(7)	$\frac{13}{2}^+$	$\frac{13}{2}^-$	5.2(4)	1.13(16)	C
230.59(2)	$\frac{23}{2}^-$	$\frac{21}{2}^+$	37.2(9)	0.64(2)	B
235.86(3)	$\frac{13}{2}^+$	$\frac{11}{2}^-$	15.0(7)	0.69(4)	D
246.04(2)	$\frac{25}{2}^+$	$\frac{23}{2}^+$	4.9(2)	0.89(7)	A
250.72(1)	$\frac{19}{2}^+$	$\frac{17}{2}^-$	30.9(9) ^c	0.66(1)	A
	$\frac{25}{2}^-$	$\frac{23}{2}^+$	18.6(8) ^c		
253.98(1)	$(\frac{19}{2}^-)$	$\frac{17}{2}^+$	6.9(2)	0.74(17)	C
259.01(6)	$(\frac{23}{2}^-)$	$\frac{21}{2}^+$	4.3(3)	0.57(23)	C
260.50(5)	$\frac{29}{2}^+$	$\frac{27}{2}^+$	4.9(3)	1.21(12)	A
265.96(1)	$\frac{27}{2}^-$	$\frac{25}{2}^+$	23.3(3)	0.66(2)	B
268.77(3)	$\frac{17}{2}^+$	$\frac{15}{2}^-$	11.0(3)	0.68(3)	D
285.73(2)	$\frac{31}{2}^-$	$\frac{29}{2}^+$	7.5(3)	0.64(3)	B
289.09(13)	$\frac{17}{2}^+$	$\frac{13}{2}^+$	2.8(3)	0.93(14)	C
290.61(4)	$(\frac{13}{2}^-)$	$\frac{11}{2}^-$	7.7(6)	0.74(8)	D
295.45(6)	$\frac{17}{2}^+$	$(\frac{13}{2}^-)$	2.9(3)	0.99(14)	D
302.53(5) ^c	$\frac{15}{2}^-$	$\frac{13}{2}^-$	25.0(10)	1.29(3)	A

intensities, and DCO ratios deduced in the present work. Relative intensities were deduced from the total projection in the $\gamma\gamma$ matrix. Figure 1 shows the DCO ratios as a function of γ -ray energy. We may distinguish three groups of transitions: first, those with DCO ratios ≈ 1.0 ; second, those with DCO ratios ≈ 0.67 ; and third, those whose DCO ratios cannot be classified in either of these two groups. The first and second groups include some transitions which were already assigned as stretched $E2$ and $E1$, respectively, in two previous papers [8,9]. In the third group we can distinguish two subgroups, corresponding to transitions below 300 keV

and above 400 keV, respectively. We attribute the former to mixed $E2/M1$ transitions and the latter, because of their large transition energies, to stretched $E2$ transitions. Their DCO ratios should lie around 1.0 but they are, in fact, slightly smaller than 1. We attribute this lowering to differences in electronic timing between the low- and high-energy transitions, for which our data were not corrected.

The extraction of mixing ratios from DCO data has been discussed by Kabadiyski *et al.* [12,13]. Here it was applied to the specific geometry of the spin spectrometer. Figure 2 depicts as examples the cases corresponding to

TABLE I. (Continued).

E_γ (keV)	I_i	I_f	I_γ	R (DCO)	Gate(s) ^a
303.6(5) ^c	$\frac{19}{2}^-$	$\frac{17}{2}^-$	4.0(10)		
316.5 ^c	$\frac{21}{2}^+$	$\frac{17}{2}^+$	18.5(16) ^c	1.07(9)	355
316.64(1)	$\frac{15}{2}^-$	$\frac{11}{2}^-$	39.8(17) ^c	1.01(4)	D
325.04(5)	$\frac{29}{2}^-$	$\frac{27}{2}^+$	5.3(4)	0.62(5)	A
335.68(4)	$\frac{23}{2}^+$	$\frac{19}{2}^+$	4.8(4)	1.12(12)	B
341.01(1)	$\frac{11}{2}^-$	$\frac{9}{2}^-$	74.2(7)	0.88(2)	B
349.39(4)	$\frac{17}{2}^+$	$\frac{13}{2}^+$	7.0(5)	1.00(8)	D
355.23(1)	$\frac{13}{2}^-$	$\frac{9}{2}^-$	100.0(9)	1.01(3)	A
359.11(3)	$\frac{17}{2}^-$	$\frac{13}{2}^-$	57.2(38)	1.00(3)	A
359.96(7)	$\frac{19}{2}^-$	$\frac{15}{2}^-$	23.5(37)		
364.01(2)	$\frac{25}{2}^+$	$\frac{21}{2}^+$	18.4(5)	0.99(8)	B
366.37(4)	$\frac{21}{2}^+$	$\frac{17}{2}^+$	11.5(5)	1.05(7)	C
391.98(2)	$\frac{33}{2}^+$	$\frac{29}{2}^+$	6.5(2)	1.09(11)	B
396.19(3)	$\frac{23}{2}^-$	$\frac{19}{2}^-$	8.9(2)	1.07(9)	B
397.74(3)	$\frac{27}{2}^+$	$\frac{23}{2}^+$	12.8(3)	0.98(8)	A
399.31(6)	$\frac{27}{2}^-$	$\frac{23}{2}^-$	3.9(2)	0.93(21)	C
401.46(1)	$\frac{21}{2}^-$	$\frac{17}{2}^-$	18.6(3)	0.99(3)	A
407.25(3)	$(\frac{25}{2}^+)$	$\frac{21}{2}^+$	4.0(1)	1.06(20)	C
409.14(6)	$\frac{37}{2}^+$	$(\frac{33}{2}^+)$	1.9(1)	0.96(25)	B
412.30(1)	$\frac{29}{2}^+$	$\frac{25}{2}^+$	15.5(3)	0.95(5)	B
413.86(10)	$\frac{29}{2}^+$	$(\frac{25}{2}^+)$	2.2(2)	1.40(47)	C
417.78(2)	$\frac{25}{2}^+$	$\frac{21}{2}^+$	8.3(3)	0.94(8)	C
419.36(6)	$(\frac{41}{2}^-)$	$(\frac{37}{2}^-)$	2.5(1)	1.19(29)	B
431.53(10)	$\frac{31}{2}^-$	$\frac{27}{2}^-$	3.3(2)	0.71(12)	B
433.55(12)	$(\frac{37}{2}^-)$	$(\frac{33}{2}^-)$	4.9(3)	0.92(15)	B
435.42(5)	$\frac{25}{2}^-$	$\frac{21}{2}^-$	8.5(5)	0.94(8)	A
442.92(6)	$\frac{41}{2}^+$	$\frac{37}{2}^+$	2.6(2)	0.95(25)	B
450.47(3)	$\frac{31}{2}^+$	$\frac{27}{2}^+$	7.5(4)	0.90(7)	A
454.94(3)	$\frac{37}{2}^+$	$\frac{33}{2}^+$	6.8(3)	0.88(10)	C
466.27(8)	$(\frac{45}{2}^-)$	$(\frac{41}{2}^-)$	2.1(2)	1.17(42)	B
468.3(2)	$\frac{33}{2}^+$	$\frac{29}{2}^+$	6.1(2)	0.89(13)	B
472.57(18)	$\frac{29}{2}^-$	$\frac{25}{2}^-$	1.4(3)	d	
479.17(3)	$\frac{29}{2}^-$	$\frac{25}{2}^-$	5.0(2)	0.93(9)	A
485.23(8)	$\frac{33}{2}^+$	$\frac{29}{2}^+$	1.6(1)	0.94(19)	C
556.07(2)	$\frac{33}{2}^+$	$\frac{29}{2}^+$	3.4(1)	1.07(11)	A

^aIf not stated in another way, three main gates were used: A, 355+359+360; B, 317+359+360; C, 317+355; D, 366+418.

^bDoublet with $K_{\beta 2}$ x ray from Ac.

^cFrom $\gamma\gamma$ coincidences.

^dBecause of a doublet and the low intensity, it is not possible to obtain a reliable DCO value.

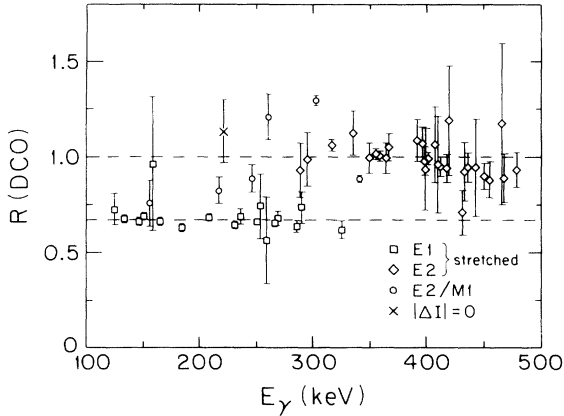


FIG. 1. DCO ratios as a function of transition energy for some selected transitions. See Table I for actual values. Dashed lines indicate the predicted values of 1.0 and 0.67 for stretched $L = 2$ and 1 transitions.

the 341, 246, 222, and 209 keV transitions. It should be noted that the dependence of the DCO ratios on the mixing ratios is itself sensitive to the alignment of the initial state. This dependence can be characterized by an attenuation coefficient α_2 as discussed in Ref. [12]. In most experiments, including the present one, α_2 is not determined. Instead, we estimated α_2 from the dispersion of the m_j distribution in the entry state which was obtained from fusion evaporation calculations using the PACE2 [14] code and by estimating the loss of alignment along the continuum and discrete cascades feeding the states studied [12]. Comparison with the experimental DCO ratios gives us the mixing ratio $\delta(E2/M1)$. The results of this analysis will be discussed in Sec. IV C.

III. LEVEL SCHEME

Figure 3 shows the level scheme derived from the present data, and Fig. 4 displays selected gated spectra showing some of the transitions discussed below. In gen-

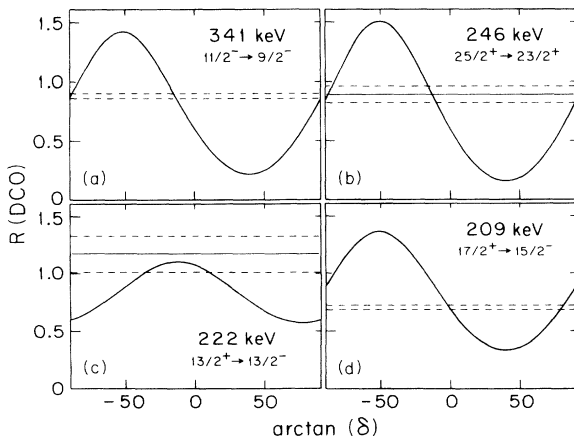


FIG. 2. Theoretical DCO ratios for some transitions as a function of the $\arctan(\delta)$, where δ is the $E2/M1$ mixing ratio. The experimentally determined mixing ratios are indicated by dashed horizontal strips.

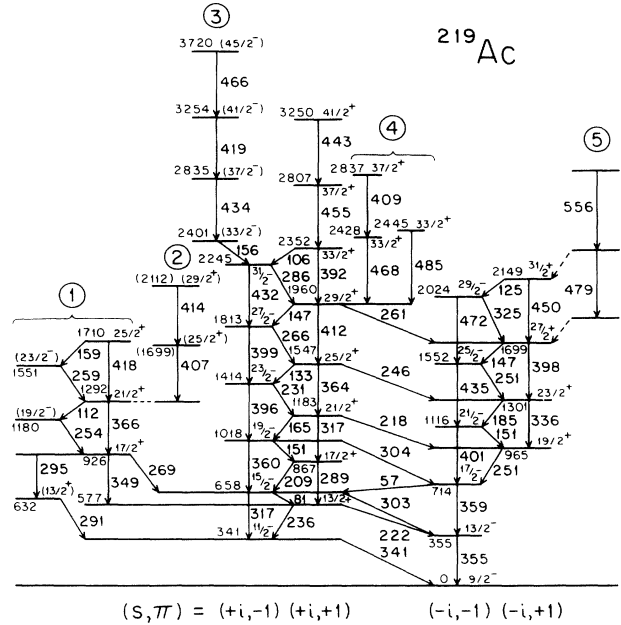


FIG. 3. Level scheme of ^{219}Ac as obtained in the present work. Transition energies are indicated in keV. See text for the meaning of dashed lines.

eral, we confirm the level scheme by Khazrouni *et al.* [9]. We confirm the 289 keV $\frac{17}{2}^+$ to $\frac{13}{2}^+$ transition reported by Ref. [9], but which was not assigned in Ref. [8]. The measured DCO ratio of 0.94(14) strongly suggests that it is a stretched $E2$ transition.

Another significant difference with Ref. [8] is associated with sideband 1 (left-hand side of Fig. 3). They placed a 535–668 keV γ cascade on top of the 926 keV $\frac{17}{2}^+$ level. We do see this cascade in our data. We find, however, that a gate on the 236 keV $\frac{13}{2}^+$ to $\frac{11}{2}^-$ transition is in coincidence with the 349.4, 366, and 418 keV transitions, while gates on the 535 and 668 keV transitions are in coincidence with a 348.5 keV transition but not with the 236 and 269 keV transitions. We have been unable to place the 348.5, 535, and 668 keV transitions in our level scheme and suspect that they are not associated with ^{219}Ac .

The additional sideband 1 observed in ^{219}Ac also has high-energy $E2$ transitions. However, the low-energy transitions (254, 112, 259, and 159 keV) do not show the strong intensity relative to the nearby $E2$'s characteristic of the low-energy $E1$'s in the other bands. Since there is no way to obtain cuts on $E2$ transitions with good statistics for these transitions, their DCO values have large error bars (Fig. 1) which preclude a definite multipolarity assignment for the low-energy transitions. Two of them are members of weak doublets (111–112 and 159–160 keV), which makes their evaluation more difficult. Adding cuts on the 418 and 366 keV lines allows one to determine DCO ratios for the 349, 295, and 291 keV lines. These cuts suggest that the 295 keV transition is of stretched $E2$ character. The DCO ratio of 0.74(8) for the 291 keV line characterizes it as a $|\Delta I| = 1$ transition corresponding to an $E1$ transition between states

of opposite parity. The linking between sidebands 2 and 1 has been indicated by a dashed line. The 414 and 407 keV transitions of sideband 2 are in coincidence with the 366 keV transition of sideband 1 but not with the 112 and 254 keV transitions. No direct interband transitions were observed. Therefore the placement of the 407 and 414 keV transitions is tentative.

In previous publications [8,9] these bands have been organized according to their simplex quantum numbers [5]. For purposes of comparison, we adopt this scheme here as well. It should be noted, however, that since ^{219}Ac is not a rigid reflection-asymmetric rotor, this simplex classification is only a convenient labeling scheme without theoretical justification. For an odd- A nucleus, the relation between simplex s , angular momentum I , and parity π is

$$s = +i : \frac{11}{2}^-, \frac{13}{2}^+, \frac{15}{2}^-, \dots, \quad (2)$$

$$s = -i : \dots, \frac{17}{2}^-, \frac{19}{2}^+, \frac{21}{2}^-, \dots,$$

as indicated in Fig. 3. We have extended the ($s = +i$, $\pi = +$) band by two transitions. The interpretation of the level scheme after the 2245 keV $\frac{31}{2}^-$ level is not entirely clear at present. Though the cascade 466–419–434 keV (sideband 3) is clearly in coincidence with the transitions below the 2245 keV state, the absence of additional transitions in coincidence with them and with members of other bands [especially with the ($+i$, $+$) band] makes its placement tentative. The ordering of the transitions is based on intensities. The same is true for the 156 keV line. It certainly belongs to this cascade, but its low energy and the probable $E2/M1$ character suggest that it belongs to a new structure on top of the ($s = +i$, $\pi = -$) band. The low intensity of the 156 keV line relative to the 434 keV line can be explained in terms of the large internal conversion coefficients for an $E2$ or mixed $E2/M1$ transition. The ordering of the transitions in the 409–468 keV cascade is also tentative, since it was arrived at on the basis of intensities alone. The measured DCO value of 0.71(12) for the 432 keV $\frac{31}{2}^-$ to $\frac{27}{2}^-$ transition of the (s, π) = ($+i, -$) band seems to contradict the stretched $E2$ character that we assigned to it. It should be noted, however, that this line is close to the $\frac{37}{2}^-$ to $\frac{33}{2}^-$ 434 keV transition, which makes the extraction of the DCO ratio difficult. The placement of the 2245 keV $\frac{31}{2}^-$ level is well established by means of coincidence correlations, and the $E1$ assignment of the parallel 286 and 147 keV transitions is well established through the measured DCO ratios.

On top of the ($-i, +$) band, we observe a structure denoted as sideband 5 in Fig. 3. The 556 keV line is observed in coincidence with the 450 keV transition and even more strongly with the 479 keV line. The 479 keV line is clearly in coincidence with transitions below the $\frac{27}{2}^+$ state but not with the 450, 125, and 325 keV lines. The placement of the 556 and 479 keV lines is based on these findings. The connection between sideband 5 and the ($-i, +$) band is indicated by dashed lines, even though no direct transitions between the two structures have been identified. Gamma transitions between the two

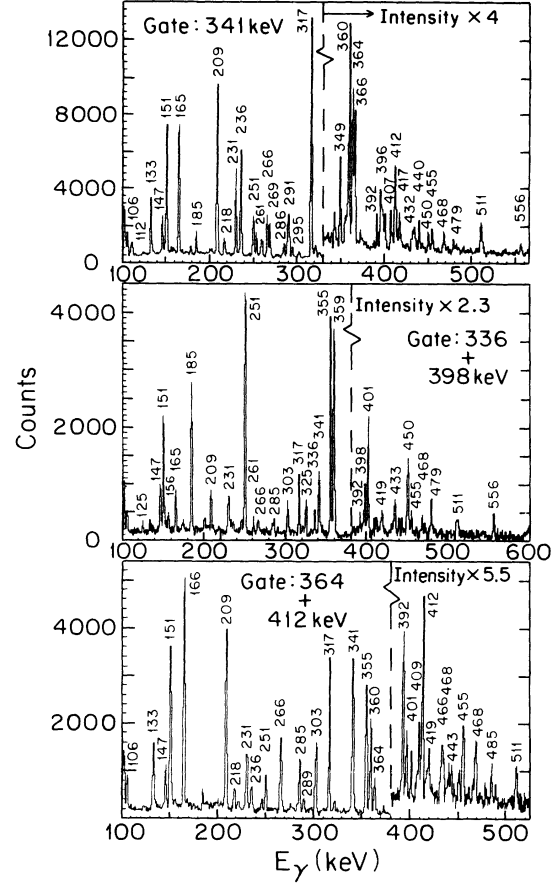


FIG. 4. Gated gamma-ray spectra. Transition energies of some of the most important transitions are indicated in keV.

structures may be strongly suppressed by competition with internal conversion if they are of low energy and $E2/M1$ character.

We do not see any direct continuation of the $s = -i$ band above the previously known $\frac{29}{2}^-$ and $\frac{31}{2}^+$ states at 2024 and 2149 keV. This is in fact a striking finding since (i) the 450 keV $\frac{31}{2}^+$ to $\frac{27}{2}^+$ transition has still a large intensity (almost 10% of the 355 keV transition from the $\frac{13}{2}^-$ state to the ground state) and (ii) the 2149 keV $\frac{31}{2}^+$ is yrast at this spin.

We observed three $E2/M1$ transitions: 218, 246, and 261 keV. The 261 keV transition linking the two positive-parity bands of opposite simplex had already been observed by Khazrouni *et al.* [9]. It is interesting to note that we observe transitions between the ($+i, -$) and the ($-i, -$) band only for $I_{\text{initial}} < \frac{19}{2}^-$, while we see transitions between the ($+i, +$) and ($-i, -$) bands up to $I_{\text{initial}} = \frac{29}{2}^+$. Thus the question arises whether this difference is associated with differences in the $\pi = -$ and $\pi = +$ structures (Fig. 4).

IV. ANALYSIS AND DISCUSSION

A. Excitation spectrum

It is experimentally [8] and theoretically [1–6] well established that ^{219}Ac is in the transition region between

the light actinium isotopes, which can be interpreted in terms of the spherical shell model, and the heavier isotopes, which are highly collective in both the quadrupole and octupole degrees of freedom. The transition between the two regimes takes place around neutron number $N = 130$. It should be noted that the isotopes of ^{88}Ra [15–21], ^{89}Ac [8,9,22–24], and ^{90}Th [25–27] show the same qualitative transition in the quadrupole deformation when going from $N = 129$ to 132 [1]. The excitation spectra of nuclei with $N < 130$ can be interpreted up to the highest spins known in terms of multiparticle shell model configurations. For example, in ^{217}Ra [16] with $N = 129$, all observed states up to the $\frac{29}{2}^+$ state at 2301 keV have been associated with the neutron excitations $\nu(g_{9/2})^3$, $\nu(g_{9/2}^2, i_{11/2})$, and $\nu(i_{11/2}^2, g_{9/2})$. The latter configuration corresponds to the maximally aligned $\frac{29}{2}^+$ state. Higher excited states are more complex involving proton excitations to $h_{9/2}$, $f_{7/2}$, and $i_{13/2}$ shells, in addition to neutron $j_{15/2}$ excitations. As discussed below, the situation in ^{217}Ac is similar. The excitation spectra of heavier nuclei with $N \geq 132$ differ drastically from those with $N < 130$. These nuclei show appreciable quadrupole and octupole collectivity and can be interpreted in terms of a reflection-asymmetric rotor.

In the intermediate nucleus ^{219}Ac with $N = 130$, the presence of low-energy octupole collectivity is well established by the occurrence of strong $E1$ transitions and the existence of parity doublets. But the quadrupole deformation is not yet well developed in this nucleus as shown by its quasivibrational spectrum, whereas in the next odd- A nucleus ^{221}Ac [28], both the quadrupole and the octupole collectivity are better developed. A detailed discussion of the evolution of quadrupole and octupole collectivity in the even-even Th and Ra nuclei between $N = 130$ and 140 can be found in Refs. [5,6]. It should be noted that the bandhead calculations of Ref. [4] predict the ground state of ^{219}Ac to be a spherical $h_{9/2}$ state. The low-lying excited states are predicted to be weakly deformed in some cases and spherical in others. The predicted quadrupole deformations for one-proton states are small, $\beta_2 < 0.085$. However, these small β_2 deformations are accompanied by significant octupole deformations $\beta_3 \approx 0.1$.

The calculations of Ref. [3] suggested that the $s = +i$ main bands are parity mixed, i.e., $\pi(h_{9/2} + i_{13/2})$, while the main component of the ground band ($s = -i$ in Fig. 3) and band 1 are pure $h_{9/2}$. These early calculations are in general agreement with the more recent calculations of Ref. [4]. The latter, however, describe the ground band

and band 1 in terms of a mixed proton configuration $\pi(h_{9/2} + f_{7/2} + i_{13/2})$. (The quadrupole deformation leads to the strong mixing of the $h_{9/2}$ and $f_{7/2}$ orbitals.)

The most surprising finding of the present experiment pertains to the upper part of the main bands. The previously established quasivibrational structure [8,9] of the $(+i, +)$ and $(+i, -)$ bands breaks down at the $I^\pi = \frac{29}{2}^+$ state at 1960 keV and at the $\frac{27}{2}^-$ state at 1813 keV. Above these states the excitation spectrum and the decay pattern become irregular, indicating a sudden collapse of collectivity above ~ 2000 keV. It is interesting to note that these states can be understood in terms of multiparticle shell model configurations. It is very illustrative to compare the high-spin states of ^{219}Ac with the higher-lying multiparticle excitations in neighboring noncollective nuclei with $N < 130$. Table II summarizes some of the striking similarities between ^{219}Ac , ^{217}Ac , and ^{215}Fr . The first entry for each state is the excitation energy in keV. The second entry represents, where available, the lifetime of the state in nanoseconds. The last column lists shell model configurations based on the calculation of Ref. [29] for ^{215}Fr . Note that the states selected for this comparison have been identified to correspond to the optimal stretched configurations in ^{215}Fr . The experimentally determined very long lifetimes, where available, are consistent with the few-particle excitation picture for these states. Lifetime measurements in ^{219}Ac both below and above the transition region at 2000 keV could provide important insight into the rapidity of this transition and the degree of collectivity at low excitation energy.

The two $s = -i$ bands seem to terminate at $I = \frac{29}{2}^-$ and $\frac{31}{2}^+$, respectively. This appears to be in conflict with the large intensity of the 450 keV $\frac{31}{2}^+ \rightarrow \frac{27}{2}^+$ transition (almost 10% of the 355 keV transition), though, as mentioned earlier, structure 5 shown in Fig. 3 does feed the $(-i, +)$ band, but no direct feeding transitions have been observed. Such transitions may be highly converted if they correspond to $M1$ and/or $E2$ transitions of low energy. It should be pointed out that there is a striking similarity between the $s = -i$ bands and band 5 and the excitation spectrum of the neighboring odd $N = 130$ nucleus ^{217}Fr [30]. This is illustrated in Fig. 5. In ^{217}Fr , the $(-i, +)$ band has been tentatively observed up to the $\frac{39}{2}^+$ state. A structure very similar to that of band 5 in ^{219}Ac was also identified, and direct feeding transitions to the $(-i, +)$ band were identified.

An additional interesting feature is sideband 1. Refer-

TABLE II. Similarities between ^{215}Fr [29], ^{217}Ac [22], and ^{219}Ac [8,9] (and present work). First entry for each nucleus is the excitation energy in keV; second entry is lifetime in nanoseconds. Configurations are based on Ref. [29] for ^{215}Fr .

I^π	$^{215}\text{Fr}_{128}$	$^{217}\text{Ac}_{128}$	$^{219}\text{Ac}_{130}$	Configuration
$\frac{27}{2}^-$	1813;3(2)	1917	1813	$\nu(g_{9/2}, i_{11/2})\pi f_{7/2}$ stretched
$\frac{29}{2}^+$	2016;8(2)	2013;740(40)	1960	$\nu(g_{9/2})^2, \pi i_{13/2}$ stretched
$\frac{33}{2}^+$	2251;8(2)		2352	$\nu(g_{9/2}, i_{11/2})\pi(i_{13/2})$ stretched
$\frac{41}{2}^-$	3207		3254	$\nu(g_{9/2}, i_{11/2})\pi(h_{9/2})$ stretched

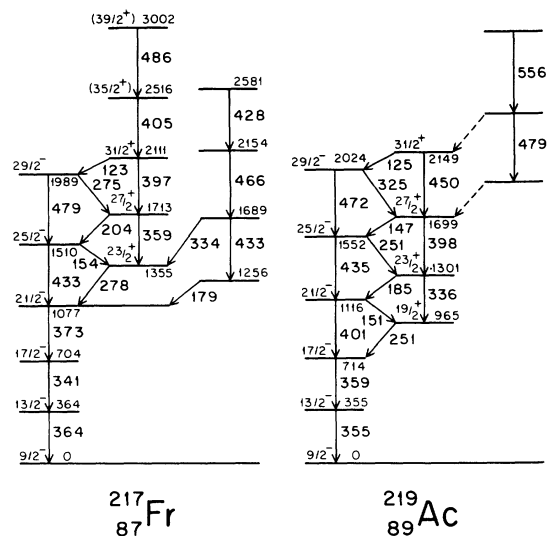


FIG. 5. The $s = -i$ bands in ^{219}Ac and ^{217}Fr [30].

ence [4] predicts an $i_{13/2}$ proton level at 475 keV. It can most likely be associated with one of the two $\frac{13}{2}^+$ states at 577 and 632 keV. These two states are probably mixed since they lie close in energy and both communicate with the $\frac{17}{2}^+$ level at 926 keV and the $\frac{11}{2}^-$ level at 341 keV. The large intensity of the 349 keV transition between the $\frac{17}{2}^+$ and $\frac{13}{2}^+$ states suggests that the latter is the bandhead of sideband 1. The 289 keV transition between the $\frac{17}{2}^+$ state of the $(+i, +)$ band and the $\frac{13}{2}^+$ state is much weaker and should probably be interpreted as an interband transition between the $(+i, +)$ band and sideband 1, making the $\frac{17}{2}^+$ state at 867 keV the bandhead of the $(+i, +)$ band.

The only other odd- A nucleus in this region where a sideband similar to band 1 has been observed is ^{219}Ra [21]. The nearby odd-odd nucleus ^{220}Ac [24] also shows a sideband with similar transition and excitation energies. The similarities in the transition energies of these three nuclei are quite striking and might be indicative of related intrinsic structures.

B. Octupole collectivity

The $B(E1)/B(E2)$ ratios extracted from our data are shown in Fig. 6 as a function of spin. Figure 6(b) is a summary of the known $B(E1)/B(E2)$ ratios for the Ra [16,19,21,31] isotopes, ^{217}Fr [30], and ^{220}Ac [24], and Fig. 6(c) summarizes the corresponding results for the Th [25–27] isotopes. The $B(E1)/B(E2)$ ratios of ^{219}Ac show no obvious simplex dependence and no distinct pattern as a function of spin, in agreement with the behavior found in other light actinide nuclei [see Figs. 6(b) and 6(c)]. They range in value from 0.4 to $3.0 \times 10^{-6} \text{ fm}^{-2}$ (with the exception of the value at $I = \frac{31}{2}$). The $B(E1)/B(E2)$ ratios in the other light actinide nuclei scatter, with few exceptions, between the same limits [see Figs. 6(b) and 6(c)]. The similarity of the ratios in ^{219}Ac to those in ^{218}Ra [18] has been related [8] to a probable similarity in

the intrinsic structure of these nuclei. In view of the overall systematics of the $B(E1)/B(E2)$ ratios in the light actinide region, however, it does not seem possible to draw firm conclusions based on similarities or differences between these ratios (see Ref. [32] for more discussion).

The high $B(E1)/B(E2)$ values in ^{219}Ac have generally been associated with octupole deformed shapes. Such deformations might be either static or dynamic. Information concerning the nature of these deformations can be obtained from the energy displacement δE between the positive- and negative-parity bands,

$$\delta E = E(I^-) - \frac{1}{2} \{E[(I+1)^+] + E[(I-1)^+]\}, \quad (3)$$

and the rotational frequency ratios

$$\frac{\omega(I^-)}{\omega(I^+)} = \frac{E[(I+1)^-] - E[(I-1)^-]}{E[(I+2)^+] - E[(I-2)^+]}. \quad (4)$$

In the limit of stable octupole deformation [5], these two ratios should be close to 0 and 1, respectively. In Figs. 7(a) and 7(b) these two quantities are plotted as a

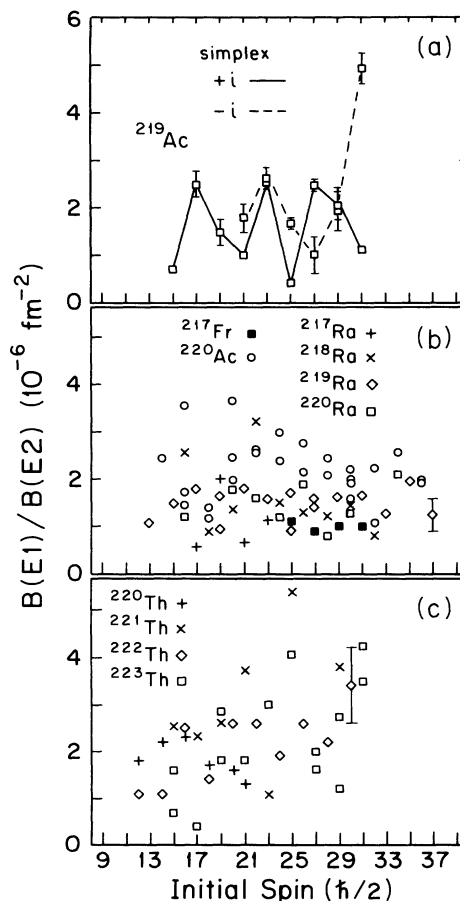


FIG. 6. Summary of $B(E1)/B(E2)$ ratios: (a) for ^{219}Ac (present work), (b) compilation of results for Ra [16,19,21,31], Fr [30], and Ac [24]. The ground-state spin of ^{220}Ac is not known, but was assumed to be $I = 2$ for plotting purposes. (c) Compilation of the results for Th [25–27]. The ground-state spin of ^{221}Th is not known, but was assumed to be $I = \frac{7}{2}$ [26] for plotting purposes. Some typical error bars are indicated in (b) and (c).

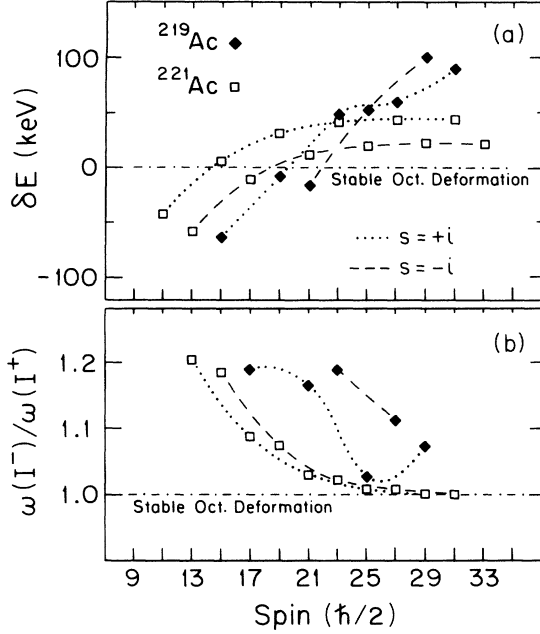


FIG. 7. Energy displacement δE between the positive- and negative-parity bands and rotational frequency ratios $\omega(I^-)/\omega(I^+)$ (see text).

function of spin for ^{219}Ac and ^{221}Ac . For ^{221}Ac both observables show a rather smooth behavior, approaching at high spin the theoretical value expected for static deformations. The values for ^{219}Ac , on the other hand, show no clear trend, indicating its transitional character.

C. Magnetic transitions

The mixing ratios $\delta(E2/M1)$ were used to derive the ratios $B(M1; I \rightarrow I-1)/B(E2; I \rightarrow I-2)$ according to

$$\frac{B(M1; I \rightarrow I-1)}{B(E2; I \rightarrow I-2)} = 0.687 \frac{I_\gamma(M1 + E2; I \rightarrow I-1)}{I_\gamma(E2; I \rightarrow I-2)} \times \frac{E_\gamma^5(I \rightarrow I-2)}{E_\gamma^3(I \rightarrow I-1)} \frac{1}{1 + \delta^2} \frac{\mu_N^2}{e^2 b^2}. \quad (5)$$

Table III summarizes these results. These ratios increase steadily with spin from about $0.02 \mu_N^2/e^2 b^2$ to $0.12 \mu_N^2/e^2 b^2$ at $I = \frac{29}{2}$, presumably indicating the loss in collectivity as the spin increases. Probable $E2/M1$ transitions have been reported in other light actinium nuclei, ^{218}Ra [17], ^{219}Ra [21], and ^{220}Ac [24], at similarly high spins; however, this is the first time that mixing ratios have been obtained.

V. SUMMARY AND CONCLUSION

The level scheme of ^{219}Ac has been extended up to a tentative spin $I = \frac{45}{2}$ and an excitation energy $E_X = 3.72$ MeV. A surprising result of this investigation is that the

TABLE III. Mixing ratios $\delta(E2/M1)$ and $B(M1; I \rightarrow I-1)/B(E2; I \rightarrow I-2)$ ratios measured in ^{219}Ac in the present work.

I_i	E_x (keV)	E_γ (keV)	$\delta(E2/M1)$	$B(M1)/B(E2)\mu_N^2/e^2 b^2$
$\frac{11}{2}^-$	341	341	-0.26(2) 0.25(5) ^a	
$\frac{15}{2}^-$	658	303	-1.0(4)	0.025(10)
$\frac{21}{2}^+$	1183	218	-0.19(6)	0.048(17)
$\frac{25}{2}^+$	1547	246	-0.23(5)	0.075(4)
$\frac{29}{2}^+$	1960	261	-0.50(10)	0.116(12)

^aFrom Ref. [6], angular distribution measurement.

extended level scheme does not follow the parity doublet structure that has been established at lower energies and spins. The parity doublet structure terminates around $I = \frac{31}{2}$ and $E_X = 2.1$ MeV and breaks up into a new family of states, presumably of the particle-hole character.

Mixing ratios were derived from DCO measurements for many transitions between bands of opposite simplex and several new transitions of this type have been established. The results are interpreted in terms of the ratio $B(M1)/B(E2)$, which seems to indicate a loss of collectivity with increasing spin.

The sideband proposed in Ref. [8] was confirmed, although with some modifications. Several new transitions were established between states of this band.

The transitional nuclei ^{219}Ac and ^{219}Ra can be at low spins understood in terms of the weak coupling of the odd particle to the quadrupole and octupole soft core of ^{218}Ra . However, at higher angular momenta these quasirotational bands terminate at nearly spherical shape. It is interesting to note that such a termination of octupole and quadrupole collectivity, anticipated in Ref. [6], was, in fact, observed in the lanthanide nuclei around ^{148}Sm [32]. In this transitional nucleus (two holes in $Z = 64$, four particles outside $N = 82$), a strong competition between collective and noncollective modes has been seen. In the spin range $I \sim 18$ the ground-state band of ^{148}Sm undergoes a dramatic change in configuration, which is seen as irregularities in level spacing. The calculations of Refs. [33,34] interpret this change as a shape transition to a noncollective structure associated with several optimal particle-hole configurations built upon $i_{13/2}$, $f_{7/2}$, and $h_{9/2}$ neutron states.

ACKNOWLEDGMENTS

The Pittsburgh group was supported by NSF Grant No. PHY-9022196. The Oak Ridge National Laboratory is managed for the U.S. Department of Energy by Martin Marietta Energy Systems, Inc. under Contract No. DE-AC05-84OR21400. The Joint Institute for Heavy Ion Research has as member institutions the Uni-

versity of Tennessee, Vanderbilt University, and the Oak Ridge National Laboratory; it is supported by the members and by the Department of Energy through Contract No. DE-FG05-87ER40361 with the University of Tennessee. Theoretical nuclear physics research at the University of Tennessee is supported by the U.S. Department

of Energy through Contract No. DE-FG05-93ER40770. S.M.F. was supported by the Notre Dame NSF Grant No. PHY90 06246. M.K.K. thanks Professor K. P. Lieb for financial support. The authors wish to thank the staff of the ORNL Holifield Heavy Ion Research Facility for their assistance.

-
- [1] I. Ahmad and P. A. Butler, *Annu. Rev. Nucl. Part. Sci.* **43** (to be published).
- [2] G. A. Leander and R. K. Sheline, *Nucl. Phys.* **A413**, 375 (1984).
- [3] G. A. Leander and Y. S. Chen, *Phys. Rev. C* **35**, 1145 (1987); **37**, 2744 (1988).
- [4] S. Cwiok and W. Nazarewicz, *Nucl. Phys.* **A529**, 95 (1991); *Phys. Lett. B* **224**, 5 (1989).
- [5] W. Nazarewicz and P. Olanders, *Nucl. Phys.* **A441**, 420 (1985).
- [6] W. Nazarewicz, G. A. Leander, and J. Dudek, *Nucl. Phys.* **A467**, 437 (1987).
- [7] A. K. Jain, R. K. Sheline, P. C. Sood, and K. Jain, *Rev. Mod. Phys.* **62**, 393 (1990).
- [8] M. W. Drigert and J. A. Cizewski, *Phys. Rev. C* **33**, 1344 (1986).
- [9] S. Khazrouni, A. Chevallier, J. Chevallier, O. Helene, G. Ramanatsizhehena, and N. Schulz, *Z. Phys. A* **320**, 535 (1985).
- [10] M. W. Drigert, K. B. Beard, U. Garg, I. Ahmad, B. Dichter, R. V. F. Janssens, T. L. Khoo, W.-C. Ma, and J. A. Cizewski, Notre Dame NSL Progress Report, 1987–1990.
- [11] J. Jääskeläinen, D. G. Sarantites, R. Woodward, F. A. Dilmanian, J. T. Hood, R. Jääskeläinen, D. C. Hensley, M. L. Halbert, and J. H. Barker, *Nucl. Instrum. Methods* **204**, 385 (1983).
- [12] M. K. Kabadiyski, K. P. Lieb, and D. Rudolph, *Nucl. Phys.* **A563**, 301 (1993).
- [13] M. K. Kabadiyski, F. Cristancho, C. J. Gross, A. Jungclauss, K. P. Lieb, D. Rudolph, H. Grawe, J. Heese, K.-H. Maier, J. Eberth, S. Skoda, W.-T. Chou, and E. K. Warburton, *Z. Phys. A* **343**, 165 (1992).
- [14] G. Gavron, *Phys. Rev. C* **21**, 230 (1974).
- [15] T. Lönnroth and C. Baktash, *Phys. Scr.* **28**, 459 (1983).
- [16] N. Roy, D. J. Decman, H. Kluge, K. H. Maier, A. Maj, C. Mittag, J. Fernandez-Niello, H. Puchta, and F. Riess, *Nucl. Phys.* **A426**, 379 (1984).
- [17] N. Schulz, V. Vanin, M. Aïche, A. Chevallier, J. Chevallier, J. C. Sens, C. Briançon, S. Cwiok, E. Ruchowska, J. Fernandez-Niello, C. Mittag, and J. Dudek, *Phys. Rev. Lett.* **63**, 2645 (1989).
- [18] M. Gai, J. F. Ennis, D. A. Bromley, H. Emling, F. Azgui, E. Grosse, H. J. Wollersheim, C. Mittag, and F. Riess, *Phys. Lett. B* **215**, 242 (1988).
- [19] Y. Gono, T. Kohno, M. Sugawahra, Y. Ishikawa, and M. Fukuda, *Nucl. Phys.* **A459**, 427 (1986).
- [20] P. D. Cottle, M. Gai, J. F. Ennis, J. F. Shriner, Jr., D. A. Bromley, C. W. Beausang, L. Hildingsson, W. F. Piel, Jr., D. B. Fossan, J. W. Olness, and E. K. Warburton, *Phys. Rev. C* **33**, 1855 (1986).
- [21] M. Wieland, J. Fernandez Niello, F. Riess, M. Aïche, A. Chevallier, J. Chevallier, N. Schulz, J. C. Sens, C. Briançon, R. Kulesa, and R. Ruchowska, *Phys. Rev. C* **45**, 1035 (1992).
- [22] D. J. Decman, H. Grawe, H. Kluge, K. H. Maier, A. Maj, N. Roy, Y. K. Agarwal, K. P. Blume, M. Guttormsen, H. Hiibel, and J. Recht, *Nucl. Phys.* **A436**, 311 (1985).
- [23] M. E. Debray, M. Davidson, A. J. Kreiner, J. Davidson, G. Falcone, D. Hojman, and D. Santos, *Phys. Rev. C* **39**, 1193 (1989).
- [24] N. Schulz, V. R. Vanin, A. J. Kreiner, E. Ruchowska, M. Aïche, C. Briançon, A. Chevallier, J. Chevallier, M. E. Debray, and J. C. Sens, *Z. Phys. A* **339**, 325 (1991).
- [25] W. Bonin, H. Backe, M. Dahlinger, S. Glienke, D. Habs, E. Hanelt, E. Kankeleit, and B. Schwartz, *Z. Phys. A* **322**, 59 (1985).
- [26] M. Dahlinger, E. Kankeleit, D. Habs, D. Schwalm, B. Schwartz, R. S. Simon, J. D. Burrows, and P. A. Butler, *Nucl. Phys.* **A484**, 337 (1988).
- [27] D. Ward, G. D. Dracoulis, J. R. Leigh, R. J. Charity, D. J. Hinde, and J. O. Newton, *Nucl. Phys.* **A406**, 591 (1983).
- [28] N. Schulz, Proceedings of the XXVII Zakopane School of Physics, Zakopane, Poland, *Acta Physica Polonica B* **24**, 23 (1993).
- [29] N. Schulz, S. Khazrouni, A. Chevallier, J. Chevallier, L. Kraus, I. Linck, D. C. Radford, J. Dudek, and W. Nazarewicz, *J. Phys. G* **10**, 1201 (1984).
- [30] M. Aïche, A. Chevallier, J. Chevallier, S. Hulne, S. Khazrouni, N. Schulz, and J. C. Sens, *J. Phys. G* **14**, 1191 (1988).
- [31] A. Celler, C. Briançon, J. S. Dionisio, A. Lefebvre, C. Vieu, J. Zylicz, R. Kulesa, C. Mittag, J. Fernandez-Niello, C. Lauterbach, H. Puchta, and F. Riess, *Nucl. Phys.* **A432**, 421 (1985).
- [32] P. Butler and W. Nazarewicz, *Nucl. Phys.* **A533**, 249 (1991).
- [33] W. Urban *et al.*, *Phys. Lett. B* **258**, 293 (1991).
- [34] W. Nazarewicz and S. L. Tabor, *Phys. Rev. C* **45**, 2226 (1992).